THE ASTROPHYSICAL JOURNAL, 512:145–156, 1999 February 10

THE MISDIRECTED CENTRAL ENGINE OF THE HYPERLUMINOUS INFRARED GALAXY AND TYPE 2 QSO IRAS P09104+4109[1,2]

DEAN C. HINES AND GARY D. SCHMIDT
Steward Observatory, University of Arizona, Tucson, AZ 85721; dhines@as.arizona.edu, gschmidt@as.arizona.edu
BEVERLEY J. WILLS
Astronomy Department and McDonald Observatory, University of Texas, Austin, TX 78712; bev@panic.as.utexas.edu
PAUL S. SMITH
National Optical Astronomy Observatories,[3] P.O. Box 26732, 950 North Cherry Avenue, Tucson, AZ 85726-6732; psmith@noao.edu
AND
LOUIS G. SOWINSKI
Steward Observatory, University of Arizona, Tucson, AZ 85721; gsowinski@as.arizona.edu
Received 1998 April 29; accepted 1998 September 17

ABSTRACT

Hubble Space Telescope Wide-Field Planetary Camera 2 imaging polarimetry of the hyperluminous infrared galaxy (and misdirected QSO) IRAS P09104+4109 reveals a highly polarized ($p \approx 20\%$) giant (~ 5 kpc) bipolar reflection nebula centered on the nucleus. This, together with our previous detection of broad, polarized Mg II and newly detected broad, polarized Balmer emission lines in our ground-based spectropolarimetry, confirms that the lobes of the nebula are dominated by scattered light from the misdirected QSO and that the object would be indistinguishable from typical luminous QSOs if viewed from either pole. Comparison with previously published narrowband images in the light of [O III] $\lambda\lambda$4959, 5007 and [O II] λ3727 shows that the northern lobe of the nebula is coincident with the ionization cone, thus the same light that impinges on the scattering material also ionizes the narrow-line gas. The biconical structure and high polarization suggest that the central UV continuum source is surrounded by a dusty torus of half-opening angle $\sim 23^\circ$ inclined $\sim 37^\circ$ with respect to our line of sight. The radio structure of this radio-intermediate object also indicates a long-lived axisymmetry to the central power source, but with a different axis relative to the scattering bicone. We propose that this difference in axes betrays the history of a cataclysmic event that altered the fundamental orientation of the central engine—the bicone defines the current axis of the system. Radio-emitting plasma is beginning to move outward along this new axis, depriving the old radio lobes of power. IRAS P09104+4109 is the first radio-quiet/intermediate object of QSO luminosity and hidden broad lines to show direct evidence that the axisymmetric torus inferred to exist in many Seyfert nuclei is also present in objects of high luminosity.

Subject headings: galaxies: individual (IRAS P09104+4109) — galaxies: peculiar — infrared: galaxies — polarization — quasars: individual (IRAS P09104+4109)

1. INTRODUCTION

Nonstellar activity has long been known to occur in the nuclei of galaxies, but the fundamental nature and structure of the central engine(s) are still uncertain. The study of active galactic nuclei (AGNs) has relied heavily on classifications that are based on properties defined over restricted wavelength ranges. Objects are classified as Seyfert galaxies, low-ionization emission-line region galaxies (LINERS), hyperluminous infrared galaxies, quasi-stellar radio sources (quasars), quasi-stellar objects (QSOs), broad- or narrow-line radio galaxies, BL Lac objects, and so on. This bewildering array of categories is reminiscent of stellar astronomy before the H-R diagram. However, within the last 15 yr, expanded wavelength coverage and new observing techniques have enabled us to move beyond simple taxonomy toward a more fundamental understanding of the physics that drives the AGN phenomenon.

1.1. *The Dusty Torus Model for NGC 1068 and Seyfert Unification*

The discovery of a highly polarized, broad emission-line (type 1) spectrum in the otherwise narrow-lined (type 2) Seyfert galaxy NGC 1068 led Antonucci & Miller (1985) to suggest that this object contains a typical type 1 Seyfert nucleus that is obscured from our direct view by optically and geometrically thick material, possibly distributed in a torus. Light escaping along oblique paths is polarized by scattering and provides an alternate, unobstructed view of the nucleus. The presence of the hidden nucleus is also evidenced by the cone-shaped, extended [O III] $\lambda\lambda$4959, 5007 emission region (e.g., Pogge 1988; Evans et al. 1991; Arribas, Mediavilla, & Garcia-Lorenzo 1996). Recent *Hubble Space Telescope* (*HST*) UV/optical imaging polarimetry confirms that this ionized gas and the scattering material both lie within an ionization/scattering cone illu-

[1] Based on observations with the NASA/ESA *Hubble Space Telescope* obtained at the Space Telescope Science Institute, which is operated by the Association of Universities for Research in Astronomy, Inc., under NASA contract NAS 5-26555.

[2] Portions of the observations reported in this paper were obtained at the Multiple Mirror Telescope Observatory, a facility operated jointly by the University of Arizona and the Smithsonian Institution.

[3] Operated by the Association of Universities for Research in Astronomy, Inc., under contract with the National Science Foundation.

minated by a hidden UV source (Capetti, Macchetto, & Lattanzi 1997 and references therein).

The ionization/scattering cone is cospatial with the northern radio structure (Ulvestad, Neff, & Wilson 1987), but there is no optical counterpart to the southern radio structure. However, near-IR imaging polarimetry reveals a highly polarized "bicone" centered on the radio nucleus (Young et al. 1996b; Packham et al. 1997). The southwest cone is apparently obstructed by dust within the disk of the host galaxy. The biconical structure implies that NGC 1068 would appear as a type 1 Seyfert if viewed from either of *two* directions and that the opening angle and axis of the bicone are related to the distribution of obscuring material. If the bicone geometry is defined by the torus opening, then the bicone axis also defines the torus axis, which itself may be related to the angular momentum axis of the central engine.

Subsequent studies of other radio-quiet AGNs, especially using polarimetry, have shown that a model similar to that suggested for NGC 1068 successfully explains the properties of AGNs from the low-luminosity LINER NGC 4258 (Wilkes et al. 1995) to BALQSOs (e.g., Glenn, Schmidt, & Foltz 1994; Goodrich & Miller 1995; Cohen et al. 1995; Hines & Wills 1995; Schmidt, Hines, & Smith 1997; Ogle 1997; Brotherton et al. 1997) to the most luminous active galaxies and QSOs (e.g., Wills et al. 1992; Hines & Wills 1993a; Hines et al. 1995; Goodrich et al. 1996; Wills & Hines 1997; Hines & Schmidt 1997).

1.2. *The Hidden QSO in IRAS P09104+4109*

IRAS P09104+4109 at $z = 0.442$ is one of the most powerful galaxies known, with the luminosity of a QSO ($L \sim 10^{13}\ L_\odot$ from 0.3 to 70 μm)[4] and 99% of the observed flux emitted at wavelengths longer than 1 μm. It is a cD galaxy in a rich, flattened cluster that is experiencing a cooling flow (Fabian & Crawford 1995). The galaxy was selected by its strong 60 μm emission (>0.5 Jy), yet faint optical magnitude ($V > 18$; Kleinmann et al. 1988, hereafter K88). Its "warm" far-IR color $F(25\ \mu\text{m})/F(60\ \mu\text{m}) \approx 0.3$ is similar to that of luminous optically selected QSOs and suggests that much of the far-IR emission is emitted from dust heated by the central UV continuum source (e.g., de Grijp et al. 1985; Neugebauer et al. 1986). The rest frame UV/optical spectrum of the nucleus shows a type 2 spectrum with strong, narrow emission lines covering a range of ionizations. This implies photoionization by a strong UV nonthermal continuum (K88; Soifer et al. 1996; see also Evans et al. 1998).

The ground-based [O III] $\lambda\lambda$4959, 5007 image of IRAS P09104+4109 is extended $\sim 3''$ to the north at a position angle $\theta \approx 14°$ (K88) and resembles the "ionization cone" seen in NGC 1068. Recent optical integral field spectroscopy shows that [Ne III] λ3869, Hβ, and Hα share similar extent, while [O II] λ3727 extends to at least 5″ (Crawford & Vanderriest 1996). The [O III] emission dominates the R photometric band at this redshift, so a broadband image shows the same extended structure (Hutchings & Neff 1988; Evans et al. 1998). However, R- and K-band images also reveal emission blobs projected against the stellar envelope that have colors and magnitudes consistent with the bulges of cluster galaxies (Soifer et al. 1996). Although there is no evidence in the broadband colors that the IR-emitting dust obscures the bulk of the starlight, some extinction is indicated by the narrow emission-line ratios ($A_v \sim 1.8$; Soifer et al. 1996).

As part of a polarimetric investigation of a flux-limited, color-selected *IRAS* AGN sample, Hines & Wills (1993a, hereafter HW93) looked for direct evidence of a hidden QSO nucleus in IRAS P09104+4109. Spectropolarimetry and broadband polarimetry revealed continuum polarization increasing from 4% at 7900 Å to more than 20% at 3600 Å, but the strong narrow emission lines are only slightly polarized ($\leq 1\%$). The polarization position angle is perpendicular to the extended [O III] emission. For rest wavelengths between 2500 and 4000 Å the spectrum of polarized flux is dominated by a power-law continuum and highly polarized, broad Mg II λ2800 emission with equivalent width typical for luminous QSOs (HW93; Hines & Wills 1993b). Thus, like NGC 1068, IRAS P09104+4109 contains a type 1 nucleus that is obscured from direct view but is revealed in light polarized by scattering. Following this discovery, polarized broad Mg II emission features have been found in a few high-redshift, "narrow line" radio galaxies (e.g., di Serego Alighieri, Cimatti, & Fosbury 1994) and in the hyperluminous infrared galaxy F15307+3252 (Hines et al. 1995).

In contrast to the radio-weak Seyfert galaxies, 6 and 21 cm images of IRAS P09104+4109 show a classical double-lobed morphology at a position angle of $\theta_{\rm RL} = 333°$ (probably an FR II radio source; Fanaroff & Riley 1974), but the unusually steep radio spectral indices imply that the radio lobes are no longer being actively fed by energetic particles (HW93). The similar brightness of the two radio jets suggests that they lie near the sky plane, but the flatter spectral index of the radio core, and its dominance, indicates that the core emission is still being powered and may be beamed toward us. The axis of the radio jets is not obviously related to the extended [O III] emission or to the position angle of polarization, but the 21 cm radio core shows a possible extension along the [O III] extended emission.

The hyperluminous infrared galaxies (HIGs) (Cutri et al. 1994), of which IRAS P09104+4109 is the prototype, are dominated by narrow optical emission lines but have far-IR properties that are nearly identical to the QSOs, and several have now been shown to harbor obscured type 1 nuclei that are seen only in scattered light (Hines & Wills 1993b; Hines et al. 1995; Goodrich et al. 1996; Young et al. 1996a). Moreover, the space density of infrared galaxies in the local universe with $\log (L_{\rm IR}/L_\odot) \geq 12$ is consistent with their interpretation as an important class of "unseen" QSOs (Sanders et al. 1988a, 1988b; Sanders 1992). Therefore, by analogy with Seyfert galaxies, the HIGs qualify as type 2 QSOs or "QSO-2s." At the same time, virtually all HIGs have been found to be members of interacting systems and the obscuring material might simply be debris from mergers rather than compact nuclear tori. Detection of two opposing ionization or scattering cones in HIGs with obscured type 1 nuclei would provide support for dusty nuclear tori, the bicone being formed by shadows cast by the torus and not simply by random holes in dust covering the nucleus. Such evidence has been lacking for luminous, radio-quiet QSOs.

The importance of the Seyfert analogy for QSOs and HIGs motivated us to further investigate the nuclear structure of IRAS P09104+4109. In this contribution, we

[4] We adopt a cosmology in which $H_0 = 75\ \text{km s}^{-1}\ \text{Mpc}^{-1}$ and $q_0 = 0.5$.

TABLE 1

OBSERVATION LOG

UT Date	Telescope	Instrument	Mode	Spectral Coverage	Resolution (Å)
1995 Apr 21	*HST*	WFPC2	Imaging Pol	4000–4700 Å	...
1996 Mar 17–19.....	S.O. 2.3 m	CCD SPOL	Spectropol	4000–8000 Å	8.2
1996 Dec 3–7.....	S.O. 2.3 m	CCD SPOL	Spectropol	4000–8000 Å	8.2
1996 Dec 5	S.O. 2.3 m	CCD SPOL	Imaging Pol	*B*	...
1997 Jan 22.....	MMT	Red Channel	Spectroscopic	4300–8800 Å	1.2–2.2

present new ground-based spectro- and imaging polarimetry and high-resolution imaging polarimetry obtained with *HST*. Detection of broad polarized Balmer emission lines confirms the presence of a hidden broad-line region originally identified from polarized, broad Mg II (HW93). The biconical structure for the extended polarized light seen in our *HST* images strongly supports the idea that the QSO nucleus is surrounded by a dusty torus. In the following sections we present our observations and then unravel the geometry of the scattering region and the putative nuclear torus and compare the radio axis with that of the ionization/scattering cone. We conclude with a brief discussion of the implications of our results and the dusty torus model for understanding QSOs, HIGs, and the AGN phenomenon in general.

2. OBSERVATIONS

Deep imaging polarimetry of IRAS P09104+4109 was obtained with the Wide-Field Planetary Camera 2 (WFPC2) on board *HST* using the polarizer-quad, partial rotation method (Biretta & Sparks 1995).[5] This technique utilizes a single CCD (WF2) for all exposures of a polarimetric sequence to minimize chip-to-chip variation, at the expense of nonoptimum polarizer orientations and the loss of some field of view. Four 900 s exposures were obtained in each polarizer setting using the F439W filter, a broad bandpass centered at 4300 Å ($\sim B$ band), which admits the region 2770–3190 Å in the rest frame of the galaxy. As found by HW93, this includes broad-line emission due to Mg II λ2800 plus a blue QSO-like continuum. The data frames were individually corrected for bias and flat-field response and combined into a single image for each polarizer orientation using a median of the four exposures.

The object is imaged on different parts of the chip for each polarizer quad, so the combined images were registered to 0.1 pixels using centroids of the unpolarized field galaxies. Finally, the degree and position angle of polarization were computed using a least-squares fit of the intensity modulation as a function of the polarizer angles 0°, +15°, −18°, and −33°. The results of our least-squares fit are consistent with polarimetry calculations subsequently obtained by applying the models given by Biretta & Sparks (1995). A total flux image is estimated by a summation of the four Stokes flux images. For our assumed cosmology, 1 pixel of the CCD projects to 450 pc at IRAS P09104+4109.

The *HST* data are complemented by ground-based imaging polarimetry and spectropolarimetry obtained with the 2.3 m Bok telescope of Steward Observatory and the CCD polarimeter as upgraded with a thinned, AR-coated and UV-enhanced 1200 × 800 Loral CCD. The design and use of this instrument are discussed by Schmidt, Stockman, & Smith (1992), and the data analysis parallels the description of Miller, Robinson, & Goodrich (1988). Polarimetric calibrations are made each run using a fully polarizing prism inserted into the beam, and position angles are registered to the equatorial system to better than 1° through observations of interstellar-polarized standard stars from the grid calibrated by Schmidt, Elston, & Lupie (1992). Total spectral flux is also available from the sum of the polarized spectra for each observation, using nightly calibrations of flux standards from the IRAF database obtained with the identical instrumental setups.

The spectropolarimetric results of IRAS P09104+4109 are the weighted co-addition of numerous observational sequences from two runs in 1996, obtained primarily with a 3″ wide east-west slit and an 8″ profile-weighted extraction aperture. The resulting rest frame velocity resolution is $\sim$600 km s^{-1}. The spectropolarimeter is very efficient throughout most of the optical spectral region, but declining CCD quantum efficiency and reduced throughput of the glass spectrograph elements strongly limit its performance below $\sim$4200 Å, just redward of the Mg II λ2800 emission line in the rest frame. For the ground-based polarimetric imaging, the entrance aperture of the spectrograph was opened to a 50″ × 50″ (225 kpc) square, a flat mirror replaced the grating, and the bandpass was defined by a standard *B* filter. Atmospheric seeing averaged 1.″5–2.″0 FWHM.

Finally, higher dispersion spectroscopy of IRAS P09104+4109 was obtained with the Multiple Mirror Telescope (MMT) and the Red Channel spectrograph in its cross-dispersed echellette format (Schmidt, Weymann, & Foltz 1989). A 26.°7 blaze, 150 g mm^{-1} grating operating in orders 13–7 provided continuous coverage from 4300 to 8800 Å. Although acquired under a nearly full moon, these data are sufficient to define the profiles of the prominent narrow emission lines (e.g., [O III] λ4959, 5007) at a velocity resolution of $\Delta v \sim 60$ km s^{-1} rest frame. These data are presented in the Appendix. Basic information on all of the observational material is contained in Table 1.

3. TWIN SCATTERING CONES

The spectrum given by HW93 suggests that nonstellar, highly polarized emission dominates the near-UV light of IRAS P09104+4109. The top panel in Figure 1*a* shows the *HST* total flux F439W image (2982 Å rest wavelength: *blue-white*) superposed on the Keck *K*-band image (*red*, Soifer et al. 1996) and the 21 cm radio contours (*gold*, HW93). The inset gray-scale image reveals the details of the inner regions of the *HST* image. Registration was performed by first

[5] For Biretta & Sparks (1995) see also http://www.stsci.edu/ftp/instrument_news/WFPC2/Wfpc2_isr/ wfpc2_pol_text. ps.

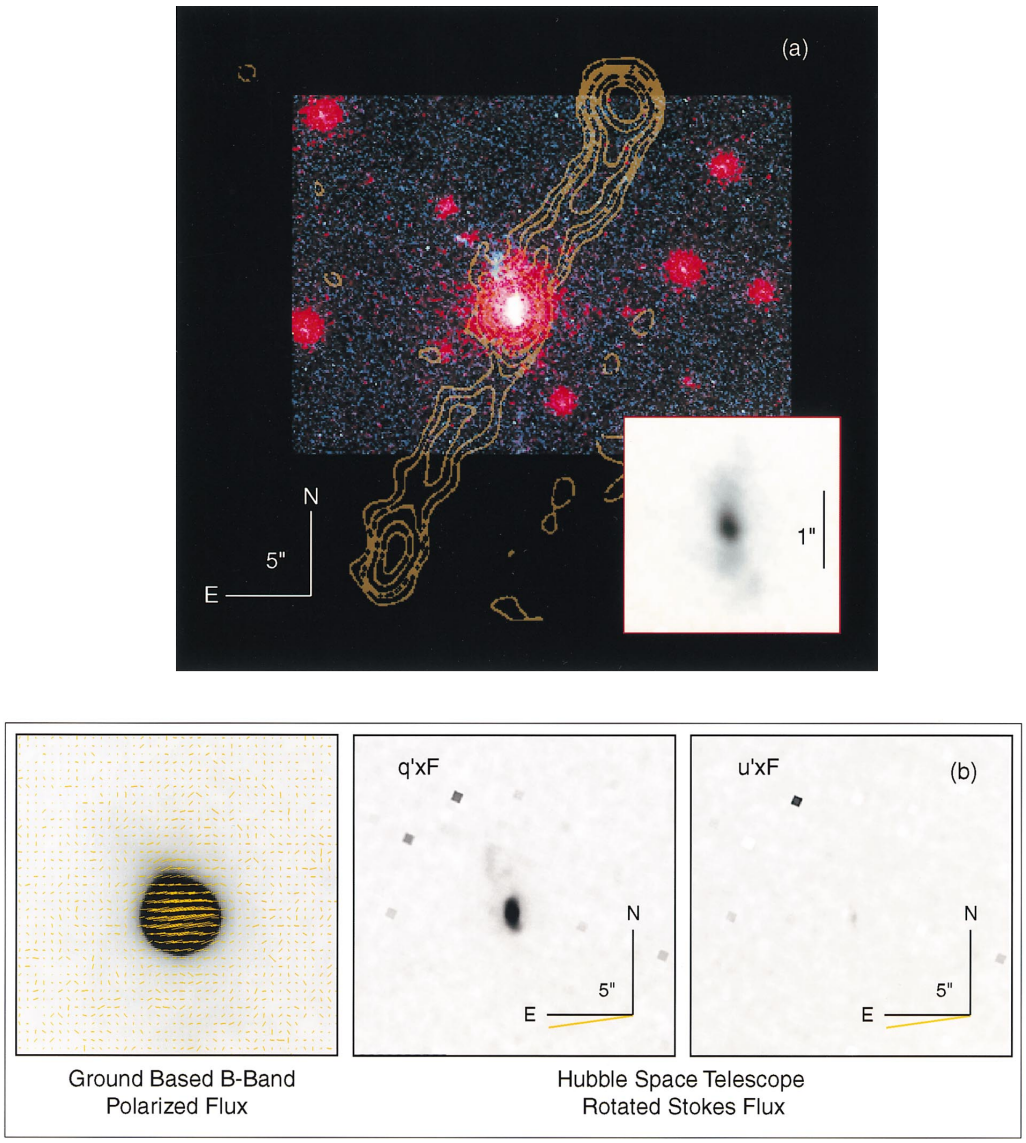

FIG. 1.—(*a*) *HST* WFPC2 (0.″1 pixel^{-1}) F439W total flux image (*blue-white*) of IRAS P09104+4109 superposed on the Keck *K*-band image (*red*, after Soifer et al. 1996) and the 21 cm radio contours from HW93 (*gold*). The images are stretched to emphasize the northern extended emission coincident with the [O III] ionization cone. The gray-scale inset presents an enlarged view of the *HST* image showing the "biconical" morphology. (*b*) Ground-based *B*-band total intensity image with the polarized intensity pseudovectors superposed in yellow (*left-hand panel*). The rotated, normalized Stokes fluxes $q' \times F$, $u' \times F$ from the WFPC2 imaging polarimetry ($q' = q \cos 2\theta + u \sin 2\theta$ and $u' = u \cos 2\theta - q \sin 2\theta$) are shown in the center and right panels. The orange lines indicate average polarization position angle $\theta = 98°$. To improve signal-to-noise ratios, the rotated Stokes parameters were constructed from images that had previously been smoothed with a 5 × 5 pixel boxcar. The majority of the flux is contained in q' confirming that the extended structure is composed almost entirely of light polarized by scattering.

aligning the 21 cm radio core with the peak of the *K*-band image and then aligning the nearby galaxies in the WFPC2 frame with the same galaxies in the *K*-band image.

Extended emission in the F439W image is visible both north and south of the central brightness peak at a position angle $\approx 11°$, with the northern emission extending into a wispy "fan" (seen as the blue extension in Fig. 1) that matches well the position angle and extent of the [O III] emission as seen from the ground (K88) and in images recently obtained with *HST* (Armus et al. 1998). The morphology of the northern extension is similar to that seen for the UV/optical scattering cone observed in NGC 1068. However, in IRAS P09104+4109 we apparently see both sides of a *bicone*.

The northern cone is brighter and falls off more slowly in intensity than the southern cone, making the central emission region somewhat egg shaped. The sharper edge on the southern end of the northern brightness peak may correspond to a region of obscuration. This morphology is strikingly similar to that of low-resolution images of the nearby, bipolar reflection nebulae CRL 2688 and M1-92 (the "Egg Nebula" and "Minkowski's Footprint"; see, e.g., Schmidt, Angel, & Beaver 1978).

The polarized flux image from our ground-based *B*-band imaging polarimetry is presented in the left-hand panel of Figure 1*b*. The overlay confirms that the polarization electric vectors are generally orthogonal to the extension in total flux, but the position angle varies slightly across the image, from $\sim 98°$ in the center to $\sim 110°$ in the northern extension. Gray-scale images of the rotated Stokes fluxes $q' \times F$, $u' \times F$ constructed from the higher spatial resolution *HST* imaging polarimetry are shown in the

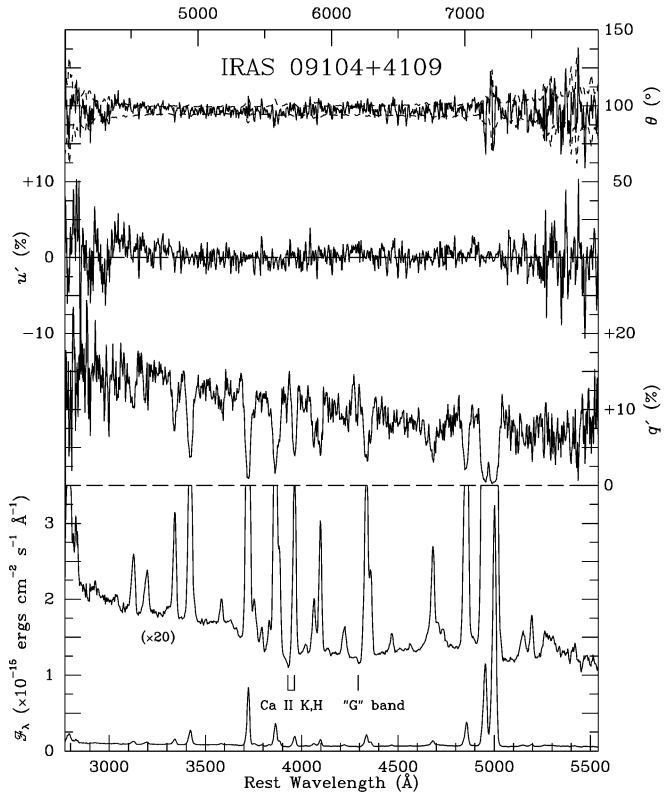

FIG. 2.—Spectropolarimetry of IRAS P09104+4109: Total flux spectrum shown at two scales (*bottom*); Stokes parameters of linear polarization q', u' for a coordinate system aligned with the overall polarization position angle of 98° (*middle two panels*); position angle of polarization θ and $\pm 1\ \sigma$ uncertainty envelope (*top*). Observed and rest frame wavelength scales are provided at top and bottom, respectively, and the flux density is in observed units of 10^{-15} ergs cm^{-2} s^{-1} Å^{-1}.

center and right-hand panels of Figure 1*b*.[6] To increase the signal-to-noise ratio, the images from each polarizer position were smoothed with a 5 × 5 pixel boxcar before they were combined into Stokes parameters. Nearly all of the flux emitted by IRAS P09104+4109 in the rest frame UV is contained in the q' image, implying that the extended emission detected in the *HST* images is highly polarized (20% ± 2%), at a position angle essentially perpendicular to the overall elongation of the source, in excellent agreement with the galaxy-corrected percentage polarization found by HW93. Even in the unbinned data, our spatial resolution is insufficient to detect polarization structure within the scattering cones.

The apparent half-opening angle of the northern cone can be measured directly from the *HST* images at $\theta_c' = 35° \pm 10°$. This angle is confirmed in higher resolution images of the ionization/scattering cone obtained with the Planetary Camera on *HST* (Armus et al. 1998). The southern cone is not as extended, but its half-opening angle appears to be consistent with the same value. This implies that the obscuring material that allows nuclear light to escape has diametrically opposed openings with approximately the same dimensions. An obscuring torus of dusty gas centered on the nucleus provides a natural geometry. In this case the axis of the scattering bicone is defined by the axis of the torus.

[6] The rotated parameters $q' = q \cos 2\theta + u \sin 2\theta$ and $u' = u \cos 2\theta - q \sin 2\theta$ ($\theta = 98°$) place all of the flux with the systemic polarization position angle into the $q' \times F$ image, and they avoid the nonnormal statistics associated with the percentage polarization P especially for lower signal-to-noise ratios (e.g., Simmons & Stewart 1985; Clarke & Stewart 1986).

4. THE SCATTERED SPECTRUM OF A QSO

HW93 found that the observed polarization of IRAS P09104+4109 is both strong and highly wavelength dependent. These characteristics are borne out by the new spectropolarimetry depicted in Figure 2. Again we present total flux and rotated Stokes components q', u' (in percentages) for a reference frame aligned with the systemic polarization position angle (depicted in the top panel of Fig. 2). The polarization of the faint continuum ($m_{\lambda 5500} = 19.3$) varies by a factor of 2—from more than 14% to 7.3%—over the range 3000–5500 Å rest wavelength. The position angle of continuum polarization is uniform within the uncertainty envelope at a value of $\bar{\theta} = 96.^\circ 7$. Strong dilution is evident at each of the major emission lines, but large swings in the polarization position angle through [O III] λλ4959, 5007 attest to a component of intrinsic polarization in these narrow features as well (see Appendix and § 5.4).

The spectrum of Stokes flux ($q' \times F_\lambda$) is displayed in Figure 3. The polarized continuum of IRAS P09104+4109 is nearly 1.5 dex bluer than its total flux spectrum ($F_\nu \propto \nu^{\alpha_\nu}$; see Fig. 5), and polarized narrow lines of Hβ and [O III] λλ4959, 5007 are evident. More important is the existence of a broad bump in polarized flux underlying narrow Hβ and a similar feature of lesser significance at the location of Hγ. The former is measured to have a rest frame equivalent width of 80 ± 25 Å and an FWHM of 12,000 ± 2500 km s^{-1}. These are well within the range of values measured for luminous QSOs (e.g., Boroson & Green 1992), and the width is consistent with the 10,000 km s^{-1} value for the Mg II λ2800 doublet in the total flux spectrum of IRAS P09104+4109 (Hines & Wills 1993b). The close similarity between the polarized flux spectrum and the type 1 spectrum of a typical quasar (Wills et al. 1999; also shown in Fig. 3) are also evident in the blue, nonstellar continuum and apparent presence of Fe II emission multiplets 7, 6, and 1 near 3200 Å rest wavelength (e.g., Grandi 1981; Wills, Netzer, & Wills 1985). These characteristics, coupled with the IR properties and twin scattering cones described above, lead us to conclude that the extended UV structure of IRAS P09104+4109 results from the light of a hidden type 1 QSO nucleus that escapes along the open poles of a dusty torus and is subsequently scattered into our line of sight.

5. STRUCTURE OF THE NUCLEUS

5.1. *Geometry of the Scattering Region and Dusty Torus*

Based on the dilution-corrected degree of polarization and an assumed conical geometry, HW93 applied a simple model appropriate for optically thin Rayleigh or Thomson scattering (Brown & McLean 1977) to derive a relation between the intrinsic half-opening angle θ_c and the inclination i of the scattering cone(s) in IRAS P09104+4109. The rather modest (dilution-corrected) polarization derived from their data (~18%) allowed for two regimes: a narrow-cone/low-inclination option or a broad cone seen at high inclination. The former was favored based on the observed morphology of the extended [O III] emission (K88).

Our direct measurement of an *apparent* half-opening angle of only $\theta_c' = 35° \pm 10°$ in the *HST* images confirms

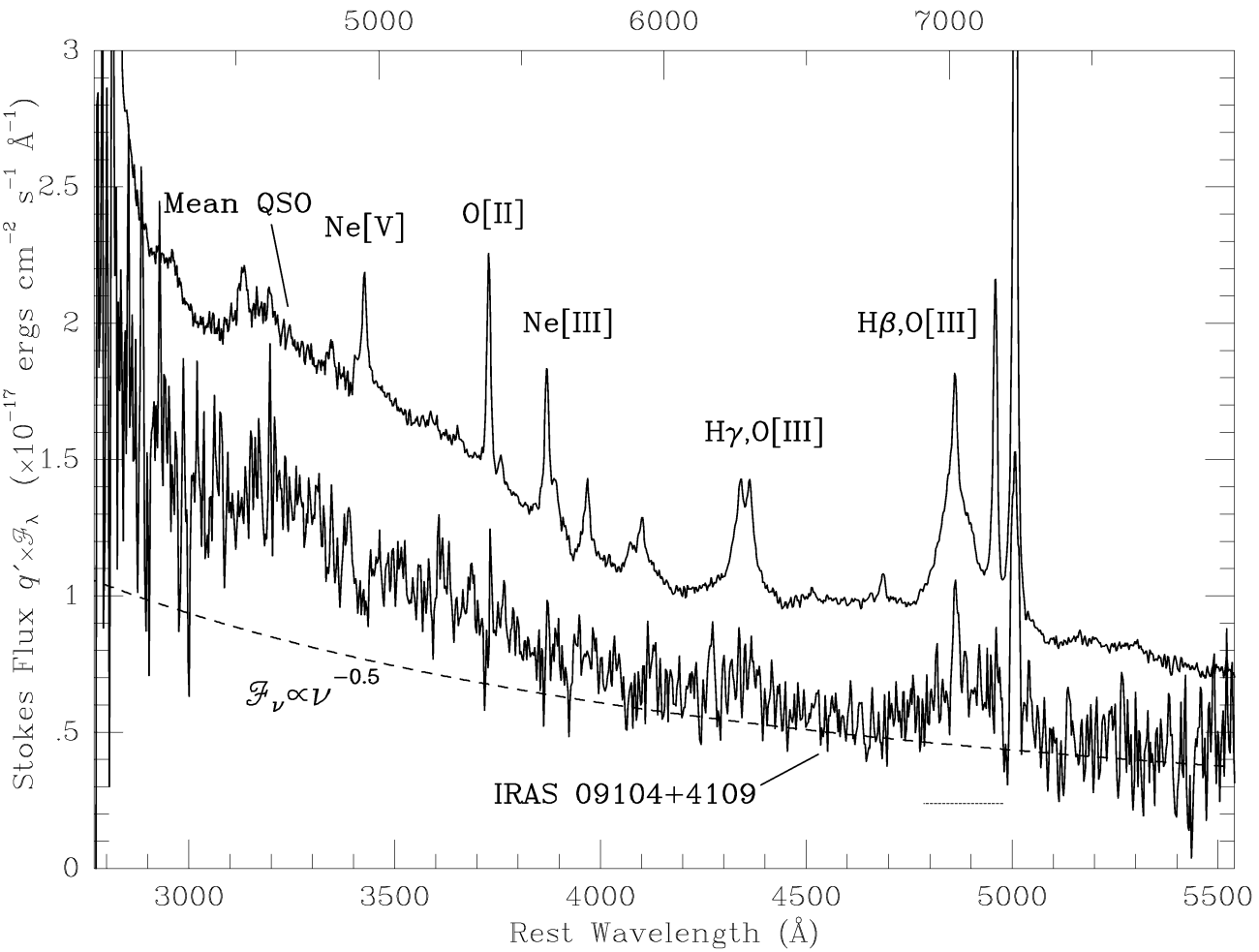

FIG. 3.—Comparison between the rotated Stokes (polarized) flux density spectrum ($q' \times F_\lambda$) of IRAS P09104+4109 and a mean radio-loud quasar spectrum (after Wills et al. 1998). The dashed curve is a power-law fit to the polarized flux density continuum in observed units of 10^{-17} ergs cm^{-2} s^{-1}Å^{-1} ($\alpha_\nu = -0.5$; $F_\nu \propto \nu^{\alpha_\nu}$). The dotted line indicates the location and FWHM of the broad Hβ emission line. Note the remarkable agreement between the polarized spectrum of IRAS P09104+4109 and the mean quasar spectrum including the similar continuum slopes, the broad-line emission from Hβ and probably Hγ, and the bump near 3200 Å associated with broad Fe II emission and Balmer continuum.

the narrow-cone option and allows us to refine the analysis of HW93. We note first that the intrinsic half-opening angle of a right cone is simply related to the observed (foreshortened) value through $\tan \theta_c = \tan \theta_c' \cdot \sin i$. This equation and the scattering model can then be solved simultaneously for the intrinsic half-opening angle (θ_c) and inclination (i), with results as summarized in Figure 4. For our measured polarization $P = 20\% \pm 2\%$ we find

$$15^\circ \lesssim \theta_c \lesssim 33^\circ \quad \text{and} \quad 34^\circ \lesssim i \lesssim 41^\circ . \qquad (1)$$

In this domain the derived parameters are rather insensitive to the intrinsic degree of polarization: if we have erred by a factor of 2 in P, the inferred values for θ_c and i change by only 6° and 16°, respectively (Fig. 4).

These results are to be compared with half-opening angles and inclinations deduced from models that seek to explain the mid- and far-IR spectral energy distribution (SED) of IRAS P09104+4109. Taniguchi et al. (1997) have used the models of Pier & Krolik (1992) to fit their recently obtained 7.1–17.3 μm ISOCAM data with a nuclear torus located 1.9 pc from the central continuum and 19 pc thick. The inferred cone half-opening angle is $\theta_c \sim 11^\circ$, and it is inclined at $i \sim 60^\circ$. However, their models account only for the mid-IR and must appeal to a cooler, more extended torus to explain the long-wavelength emission.

Granato et al. (1996) are able to explain both the mid- and far-IR SED with a single torus 0.6 pc from the central continuum and extending to 316 pc. They assume a dust density that is constant with radius but varies as a function of polar angle. While the model does not contain an explicit half-opening angle, we can define a boundary where the scattering optical depth at 0.3 μm $\lesssim 1$; light within this region can be singly scattered, producing the polarized light we observe. Their best fit to IRAS P09104+4109 suggests a half-opening angle $\theta_c \sim 30^\circ$ with inclination $i \sim 45^\circ$, in agreement with our inferred geometry (see Fig. 1; Granato et al. 1996).

5.2. *The Central Engine*

If we assume that the extremities of the scattering cones are defined by the inner walls of the obscuring torus (e.g., Storchi-Bergmann, Mulchaey, & Wilson 1992), then the covering factor of the torus is $f = \cos \theta_c = 0.84$–0.97. To this very large fraction of observers, the central engine would appear obscured and IRAS P09104+4109 would be classified as a type 2 QSO. Reprocessing of QSO light by

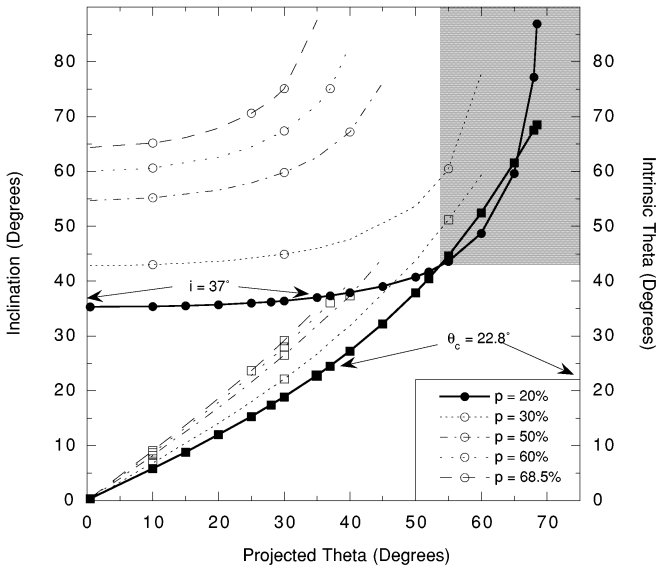

FIG. 4.—Scattering cone models (see text). For a given polarization, the models yield the inclination (*open and filled circles*) and intrinsic half-opening angle (*open and filled squares*) as a function of the projected (observed) half-opening angle of the scattering cone. We measure $p = 20\%$ and θ (projected) $= 35°$ for IRAS P09104+4109, which yields $i = 37°$ and an intrinsic half-opening angle θ (intrinsic) $\approx 23°$ (*filled circle and square*). The gray area corresponds to the condition for $p = 20\%$, where $i \leq \theta$ (intrinsic), which is ruled out since we do not see the QSO nucleus directly. Note that the maximum half-opening angle θ (intrinsic) $\approx \theta$ (projected) $\approx 70°$ is set by the polarization ($p \geq 20\%$).

dust in the torus is held responsible for the infrared excess of the object; the observed IR/optical νF_ν flux ratio is an enormous 38 between 60 and 0.55 μm (K88), more than an order of magnitude larger than that of a typical QSO with an exposed type 1 nucleus (Low et al. 1989; Cutri et al. 1994).

If we take the observed 10–100μm flux from IRAS P09104+4109 to be (isotropic) emission from a torus that is optically thick to UV-optical light from the central engine, we find the total nuclear luminosity to be $L_{\rm nuc} = 1.0 \times 10^{13}\ L_\odot$. Assuming this is powered by the 0.1–100 μm portion of a power-law continuum typical of a type 1 QSOs ($F_\nu \propto \nu^\alpha$; $-1.5 < \alpha < -0.5$), it follows that the nucleus, were it not obscured, would have a visible-light continuum flux of $F_{\rm PL} \sim 1$–5 mJy. This corresponds to $16.6 < V < 14.7$, or ~ 4 mag brighter than observed. A further implication is that, as seen from Earth, the narrow emission lines of the galaxy are overemphasized by a factor ~ 20–40 in equivalent width because of the obscuration of the nuclear continuum.

Similar to the HIG F15307+3252 (Hines et al. 1995), the inferred intrinsic ratio of $L_{\rm IR}/L_{\rm opt} \sim 3$–7 places IRAS P09104+4109 squarely among the most luminous QSOs in the $L_{\rm IR}/L_{\rm opt}$ versus $L_{\rm bol}$ diagram of Cutri et al. (1994; Low et al. 1989). We conclude that if IRAS P09104+4109 were oriented such that our view penetrated *either* open polar hole in the torus the narrow-line spectrum would be no more prominent than those seen in typical type 1 AGNs, the starlight component would be all but undetectable, and the object could have been cataloged as one of the brighter and intrinsically most luminous QSOs in the Palomar-Green sample (Schmidt & Green 1983).

5.3. *The Scattering Cones*

The consistency of the above interpretation can be checked through a comparison of the observed surface brightness of scattered light, B_s, with the inferred incident nuclear flux. For an optically thin situation, these quantities are crudely related to the scattering optical depth integrated along the line of sight by

$$\tau_s \sim 4\pi \frac{B_s}{F_{\rm inc}} \quad (2)$$

(e.g., Schmidt et al. 1978). The twin scattering cones evident in the *HST* images are dominated by the inner $\sim 1''$ ($r \lesssim 4.5$ kpc). For the ensuing solid angle, the scattered surface brightness at V is roughly $B_s \sim 2 \times 10^{-17}$ ergs cm^{-2} s^{-1} Hz^{-1} sr^{-1}. The incident flux is $F_{\rm inc} \sim (D_L/r)^2\ F_{\rm PL}$, where D_L is the luminosity distance appropriate for the adopted cosmology. We find that the optical depth to scattering averaged over the observed cones is $0.01 \lesssim \tau_s \lesssim 0.08$. Thus, the medium is found to be optically thin to scattering and the above estimates are valid.

The spectral shape of polarized flux of IRAS P09104+4109 is remarkably similar to that of the typical QSO shown in Figure 3 and is 0.4 ± 0.2 dex bluer than the residual, galaxy-subtracted total flux spectrum (see Appendix). Unfortunately, this places only mild constraints on the nature of the scattering particles. For example, if electrons were distributed uniformly throughout the cones, a number density of only 0.2 cm$^{-3} \lesssim n_e \lesssim 2$ cm^{-3} would provide the requisite optical depth and comprise an equivalent hydrogen mass of 2×10^8–$2 \times 10^9\ M_\odot$ for both cones. For gas at such low densities, the implied recombination radiation is at most a few percent of the narrow Hβ emission observed. Sparse, higher density clumps are also possible. For example, filaments with $n_e \sim 100$ cm^{-3} and a volumetric filling factor in the cones of $\sim 10^{-3}$ could also yield the observed surface brightness of scattered light without exceeding the measured narrow-line flux. Despite the fact that IRAS P09104+4109 resides within a strong cooling flow detected by *ROSAT* (Fabian & Crawford 1995), the fact that the northern scattering cone and the [O III] ionization cone are cospatial implies that hot electrons in the cooling flow are not the dominant scatterers and do not broaden the scattered emission lines.

Dust scattering by grains distributed in a uniformly filled volume can also produce a relatively unmodified emergent spectrum (e.g., Pei 1992; A. Laor 1997, private communication; see also Manzini & di Serego Alighieri 1996). Because the scattering cross section per unit mass is far larger for small grains than for electrons, the observed surface brightness of scattered light would imply much less total mass. In this case, the mild reddening implied by the narrow emission line flux ratios (Soifer et al. 1996) suggests that the gas and dust are mixed throughout the cones.

5.4. *The Kinematic and Ionization Structure of the Bicones*

As noted by K88 and seen in our MMT spectrum (see Appendix; Fig. 6), at least two kinematic components are present in the narrow emission lines. Crawford & Vanderriest (1996) spatially mapped several emission lines including [O III] λ5007 with the ARGUS integral field spectrograph on the Canada-France-Hawaii Telescope. They find that the [O III] λ5007 emission-line complex consists of two primary components with the blueshifted component constituting 32% of the total line flux and offset by -1250 km s^{-1} relative to the underlying system. The main (red) component is extended and corresponds with the extended structure seen by K88 and Hutchings & Neff

TABLE 2

NARROW-LINE POLARIZATION PROPERTIES[a]

Line and Component	Peak λ (Å)	Peak Relative Flux	$F(\mathrm{H}\beta)/F(5007)$	p (%)	σ_p (%)	Θ (deg)
[O III] λ5007:						
1.....	7201.78	0.95	0.10	0.38	0.17	152.2
2.....	7220.70	2.98	0.15	0.59	0.17	61.6
3.....	7233.99	1.02	0.15	1.44	0.17	125.5

[a] The narrow lines were unresolved and assumed widths to be that of the instrumental profile FWHM = 8.2 Å. The polarization properties of [O III] λ5007 were assumed to apply to [O III] λ4959, and narrow Hβ.

(1988), but the blueshifted component is unresolved ($\leq 0\farcs4$). Isolating those fibers that contain the red emission, Crawford & Vanderriest (1996) were able to resolve the kinematic structure into additional components with FWHM $\sim$200–1000 km s^{-1} and velocity relative to systemic of -100 to $+200$ km s^{-1}. The more redshifted components lie to the south of the nucleus and are not as extended as those to the north.

The components of the narrow-line emission also manifest themselves in our polarimetry data as the "S-shaped" position angle rotations seen across the Hβ and [O III] $\lambda\lambda$4959, 5007 emission lines.[7] Table 2 and Figure 7 present the best-fit results for modeling the polarization assuming the kinematically distinct components identified by Crawford & Vanderriest (1996).

The close correspondence between the extended emission-line gas and the scattering cones revealed by *HST* implies that the northern (blueshifted) scattering cone points toward us, while the southern (redshifted) cone points away from us; the diminished emission-line and scattered flux in the south may result from attenuation by material near the nucleus. The increased brightness of the northern radio bridge also suggests that it is associated with plasma that is directed more toward us than the southern bridge—we predict that the southern bridge will be depolarized at radio frequencies (e.g., Laing 1988; Garrington et al. 1988). The FIR emission in QSOs suggests that nuclear tori have radii $\sim$few hundred pc (e.g., Sanders et al. 1989; Mulchaey et al. 1994). If the deficit of [O III] λ5007 in the south is caused by dust extinction, this material lies at $\sim$1–4 kpc, far beyond the envisioned edge of the nuclear torus, but could still be associated with infalling material from the cooling flow or possibly stripped from nearby companion galaxies. The dark "edge" at the foot of the northern scattering cone (*inset*, Fig. 1*a*) could be the outer edge of the torus at $\sim$300 pc from the nucleus (§ 3).

The [O II] λ3727 emission is more extended than the [O III] λ5007 emission; the ionization decreases with increasing distance from the nucleus in the north. This confirms the suggestion of HW93 that their higher [O II] λ3727 flux compared with K88 resulted from observing with a larger aperture that encompassed a more extended [O II]-emitting region. The line ratios do not totally discriminate between shock excitation and photoionization, but Crawford & Vanderriest (1996) note that the ratios are consistent with photoionization dominating near the nucleus and shock excitation becoming increasingly important farther out into the extended emission.

Since the [O II] is emitted farther from the central dusty regions, it is less likely to be obscured or scattered. Therefore, as for high-redshift radio galaxies, we expect the [O II] λ3727 emission line to be less polarized than the [O III] $\lambda\lambda$4959, 5007 emission lines (e.g., di Serego Alighieri et al. 1997). Indeed this appears to be the case (H. D. Tran 1995, private communication).

6. SIGNIFICANCE OF THE BICONE

We have confirmed that IRAS P09104+4109 contains a type 1 nucleus that is obscured from our direct view by optically thick dust but is visible in light scattered by particles in diametrically opposed cones. This bicone implies that the scattering geometry is tied to the structure of the central engine, not simply caused by a random hole in a cocoon of obscuring material. The inferred luminosity and spectral properties of the nuclear emission indicate that the observed spectrum of the galaxy is overwhelmed by narrow emission lines only because the direct view of the brilliant nucleus is heavily extinguished. Indeed, viewed from the direction of either of the two scattering cones, IRAS P09104+4109 would be indistinguishable from a typical, luminous QSO.

We have interpreted the properties of IRAS P09104+4109 in terms of the simplest structure that is consistent with a biconical geometry—the axisymmetric torus. Perhaps most significant about this interpretation is that it implies that the nucleus possesses a dynamically important axis defined by the bicone, but one presumably shared by an accretion disk and ultimately the compact central object itself.

With this understanding, the radio properties of IRAS P09104+4109 become particularly relevant. The twin jet-lobe structures, which presumably also emanated along a preferred stable axis associated with the central engine, straddle a compact core at a position angle of $\theta_{\mathrm{RL}} = 333^\circ$ extending $\pm 11''$ ($\pm$50 kpc; K88; HW93). This is misaligned by 38° from the bicone symmetry axis ($\approx 11^\circ$) defined by the bicone and polarization position angle. Moreover, if the emission from the connecting radio jets is beamed, their similar brightness suggests a roughly edge-on orientation (HW93), in conflict with the modest inclination implied by our observations of the bicones ($i \sim 40^\circ$). This information suggests that the source axis of IRAS P09104+4109 has been altered during its history, such as might occur through a catastrophic interaction or accretion event (HW93) or by disk precession (Maloney, Begelman, & Pringle 1996). The presence of many companions (K88; Soifer et al. 1996;

[7] The position angle rotations across the Hβ and [O III] emission lines confirm that the polarization is not induced by interstellar polarization within our Galaxy.

Evans et al. 1998) and a strong cooling flow (Fabian & Crawford 1995) provide ample opportunities to alter the angular momentum of the central engine.

The extent of the radio lobes (≈ 51 kpc) implies particle travel times $\sim 10^5$–10^6 yr, but their steep radio spectra indicate that the plasma was ejected perhaps 10^8–10^9 yr ago (in the rest frame). The barely resolved 21 cm radio core exhibits a slight elongation in the general direction of the scattering cones, and it has a flatter spectrum compared with the lobes (HW93), implying a fresher supply of electrons. The straightness of the large-scale radio jets then suggests that the perturbation was either recent and sudden (so that lobes corresponding to the new orientation are only now being formed) or that the ejection of plasma is a sporadic phenomenon, possibly instigated by an accretion event. In either case, the UV radiation that ionizes the extended [O III]-emitting gas is apparently able to escape more readily than the relativistic plasma.

We detect scattered (rest frame) UV emission up to 5″ (22.5 kpc) from the central engine, so the current orientation has persisted for at least $\sim 7 \times 10^4$ yr. If radio plasma has continued to flow uninterrupted from the nucleus, then the difference in its $\lesssim 0\farcs5$ extent compared with the UV scattered light suggests a bulk flow of $\sim 0.1c$.

Hill & Lilly (1991) showed that about half of the powerful FR II radio galaxies at $z \approx 0.5$ inhabit rich clusters, even though similar sources avoid such environments at low redshift. The altered direction of the central engine in IRAS P09104+4109 possibly caused by interaction with inflowing cooling flow material or collisions with other cluster members (see, e.g., Hall, Ellingson, & Green 1997) may hail the transition of this object from a powerful classical double-lobed radio source to the lower (radio) power, wide-angled tail sources seen at low redshift (e.g., O'Donoghue, Eilek, & Owen 1990).

7. TYPE 2 QSOs

The success of orientation-dependent unified schemes has revolutionized our understanding of low-luminosity AGNs. There is now strong evidence that many, if not all, Seyfert galaxies contain type 1 nuclei regardless of their apparent classification (e.g., Miller & Goodrich 1990; Tran 1995). Radio-loud QSOs (quasars) and (narrow- and broad-lined) radio galaxies are also thought to share the same fundamental nuclear structure but are viewed from different angles (e.g., Barthel 1989), as are BL Lacs and FR I radio galaxies (e.g., Urry & Padovani 1995). Because of the difficulty of identifying obscured systems prior to the advent of sensitive infrared satellite surveys, the extension of the general model to luminous radio-quiet AGNs has been more problematic. However, objects such as IRAS P09104+4109 and F15307+3252 (Hines et al. 1995) now make it clear that counterparts to the obscured Seyferts can be found among the HIGs and can be effectively identified by their far-IR properties (Cutri et al. 1994; Low & Hines 1999) and perhaps their X-ray properties (e.g., Ohta et al. 1996). These objects possess the same basic geometry as their low-luminosity cousins and deserve the classification of type 2 QSO or QSO-2.

Optical surveys for QSOs are biased against highly obscured objects like IRAS P09104+4109 (Wills & Hines 1997) and thus do not contain QSO-2s, a fact that had previously motivated many authors to suggest that the torus opening angle increases with increasing luminosity (Miller & Goodrich 1990; Antonucci 1993 and references therein). While some QSOs may have large opening angles, as indicated by number counts of *IRAS*-selected QSOs and HIGs (e.g., Low et al. 1989; Cutri et al. 1994), IRAS P09104+4109 shows that there are clearly objects that possess extreme luminosities and small opening angles. Since most of the HIGs and *IRAS*-QSOs are found in strongly interacting systems (e.g., Surace et al. 1998; Hines et al. 1999), collisional debris could increase the dust cover in these objects. Over time, the active nucleus may "burn" away this debris, thus producing larger opening angles as a function of age (e.g., Sanders et al. 1988a, 1988b).

Unhindered by the relative brightness of the point source and likely viewed from higher inclinations, studies of QSO-2s from the UV through the near-infrared in the rest frame (e.g., NICMOS, NGST, and SIRTF) should provide new insights into the nature of the host galaxies, the effects of nuclear luminosity on the local environment, and the influence of mergers and encounters on the formation and evolution of QSOs. Finally, we note the crucial role that polarimetry will play in distinguishing structures dominated by scattered AGN light from those structures dominated by emission from stars, especially at higher redshifts.

We thank Christian Ready and Ray Lucas at STScI for invaluable assistance in preparation of the WFPC2 observations. R. Mark Wagner provided assistance with the MMT observations. We thank the anonymous referee for providing comments that helped to clarify the presentation. Support for this work was provided by NASA through grant number GO-5463.02-93A from the Space Telescope Science Institute, which is operated by Association of Universities for Research in Astronomy, Incorporated, under NASA contract NAS5-26555. Ground-based polarimetry at Steward Observatory receives support from the NSF through grant AST91-14087.

APPENDIX A

SPECTRAL COMPONENTS OF IRAS P09104+4109

The nearly 14 hours of integration required to obtain the polarization spectrum of IRAS P09104+4109 also yielded a total flux spectrum of extraordinarily high quality. As noted in Figures 2 and 5, absorption features from the host galaxy are present, particularly Ca II K λ3934 and the CH G band at λ4300 (Ca II H underlies Hϵ). Using the optical/*IUE* spectrum of the elliptical galaxy NGC 3379 as the stellar template (Kennicutt 1992; Oke, Bertola, & Capaccioli 1981), the starlight component was determined and subtracted (Fig. 5). Best cancellation of the stellar features was obtained for a starlight fraction $f_s = 37^{+8}_{-4}\%$ in our 3″ × 8″ extraction aperture at a wavelength of 4500 Å. No contribution from a younger stellar population, such as might arise in a recent episode of star formation, was deemed necessary. In the gaps where it can be measured, the residual continuum of the QSO is significantly bluer than that of the original spectrum, with $F_\nu \propto \nu^{-0.9}$ ($\pm \sim 0.4$ dex) for

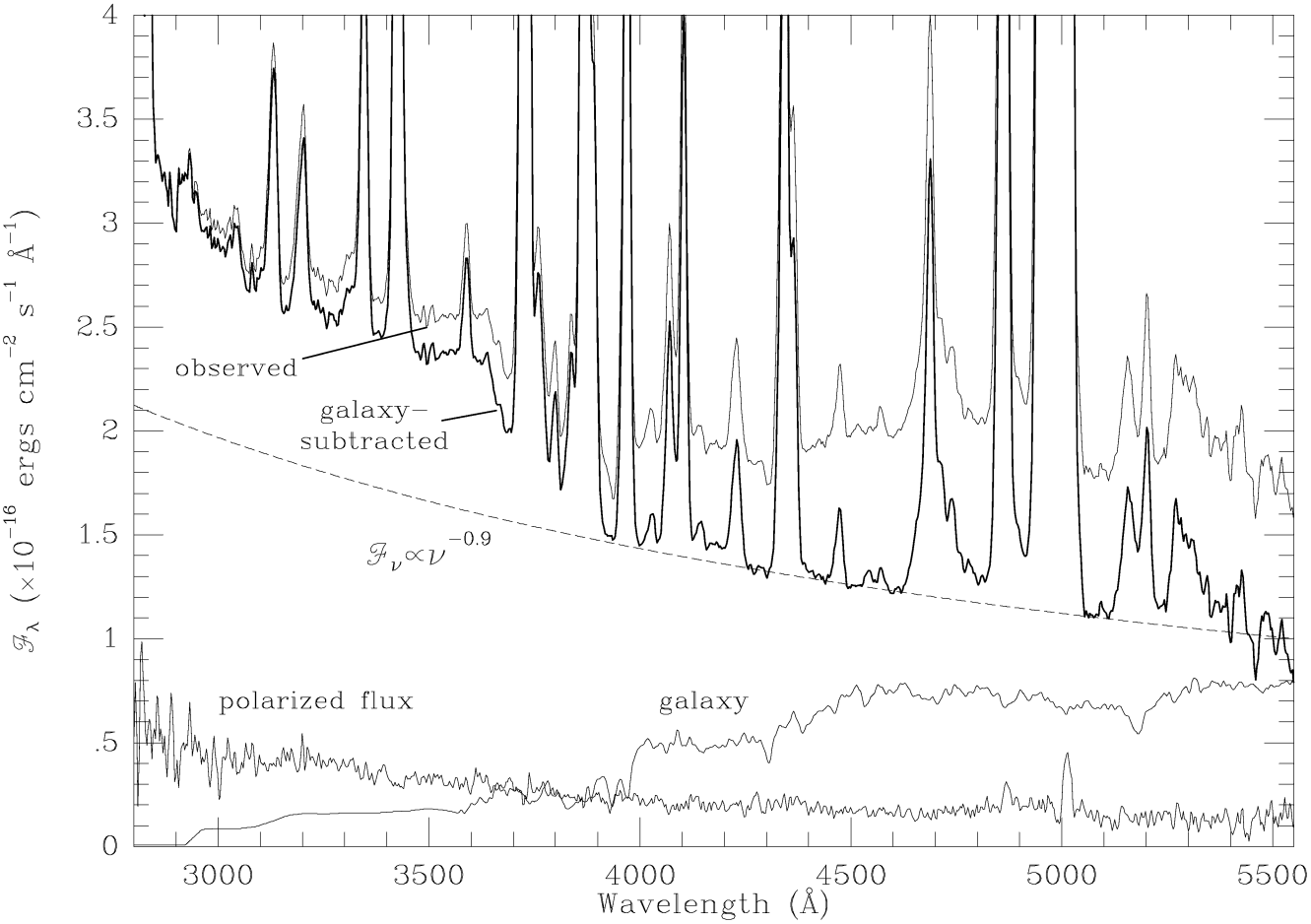

FIG. 5.—Components that make up the rest frame optical, total flux density spectrum in units of 10^{-16} ergs cm^{-2} s^{-1} Å^{-1} observed from IRAS P09104+4109. The template of the elliptical galaxy NGC 3379 (M105) from (Kennicutt 1992; Oke et al. 1981) has been scaled to match the Ca II absorption and the Balmer break of IRAS P09104+4109, consistent with 40% of the continuum at 5500 Å rest originating from old stars. The galaxy-subtracted spectrum is well fitted by a single power-law continuum ($F_\nu \propto \nu^{-0.9}$) plus narrow emission lines and, importantly, the Balmer continuum. The ratio of the rotated Stokes flux density to the fitted continuum power law yields approximately wavelength-independent polarization $p = 15\%$–22% in close agreement with that derived by HW93.

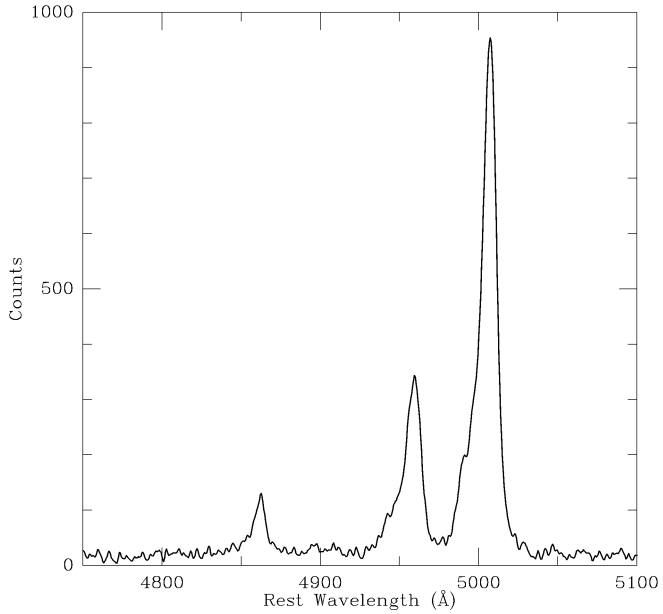

FIG. 6.—MMT spectrum in the Hβ/[O III] $\lambda\lambda$4959, 5007 region of IRAS P09104+4109 observed with a rest frame velocity resolution of $\sim$ 60 km s^{-1}

$\lambda_{\rm rest} = 3900$–$5500$. This is in good accord with the spectral slope of a typical unobscured QSO (e.g., Wills et al. 1998; Francis et al. 1992). The Balmer continuum and blue bump dominate at shorter wavelengths, in obvious resemblance to the mean quasar spectrum shown in Figure 3. Relative to the galaxy-subtracted spectrum, the polarized flux indicates an intrinsic polarization for the scattered continuum in the range $p = 15\%$–22%, essentially constant with wavelength.

The existence of two components to the [O III] λ4959, 5007 lines has been known for several years (K88; Hutchings & Neff 1988); the blue-shifted features can be distinguished as profile asymmetries in the MMT echellette spectrum shown in Figure 6. The primary (red) component was found by Crawford & Vanderriest (1996) to show velocity structure at the 100–200 km s^{-1} level, with the receding gas clouds apparently located in the southern cone. These complexities are not well resolved in the lower resolution data from the spectropolarimeter, but the expanded display of Stokes spectra for the Hβ/[O III] region in Figure 7 clearly shows that three components to each narrow emission line are required: a principal component with $q < 0$, $u > 0$, a receding component with $q < 0$, $u < 0$, and a feature that is approaching us relative to the main component by $\sim$800–900 km s^{-1} and has $q > 0$, $u < 0$. We have subjected the spectra of polarized and total flux to a least-squares analysis to solve for the central wavelengths, polarization properties, and flux ratios of the three components, with the results also shown in Figure 7. All profiles were assumed to be Gaussians with the instrumental width of 8.2 Å in order to better constrain the problem. An excellent match to the complex polarimetric behavior through the [O III] complex is achieved by the best-fit values. The fit is not as good at Hβ. This can be attributed to the underlying scattered broad-line component, which is strongly polarized at $\theta \sim 100^\circ$ and thus contributes primarily in the direction of $-q$.

The derived polarization properties summarized in Table 2 reveal that the various narrow emission-line components are only weakly polarized, ranging from 0.4% for the approaching feature to 1.4% for the receding component. While scattering may still contribute to the values measured, polarization by transmission through an intervening medium of aligned grains is also a viable mechanism and would perhaps better explain the stronger polarization from the rear (southern) scattering cone (see, e.g., Goodrich 1992). It might then be interesting to speculate on the position angle differences between the components, including the 90° rotation between the main and approaching features.

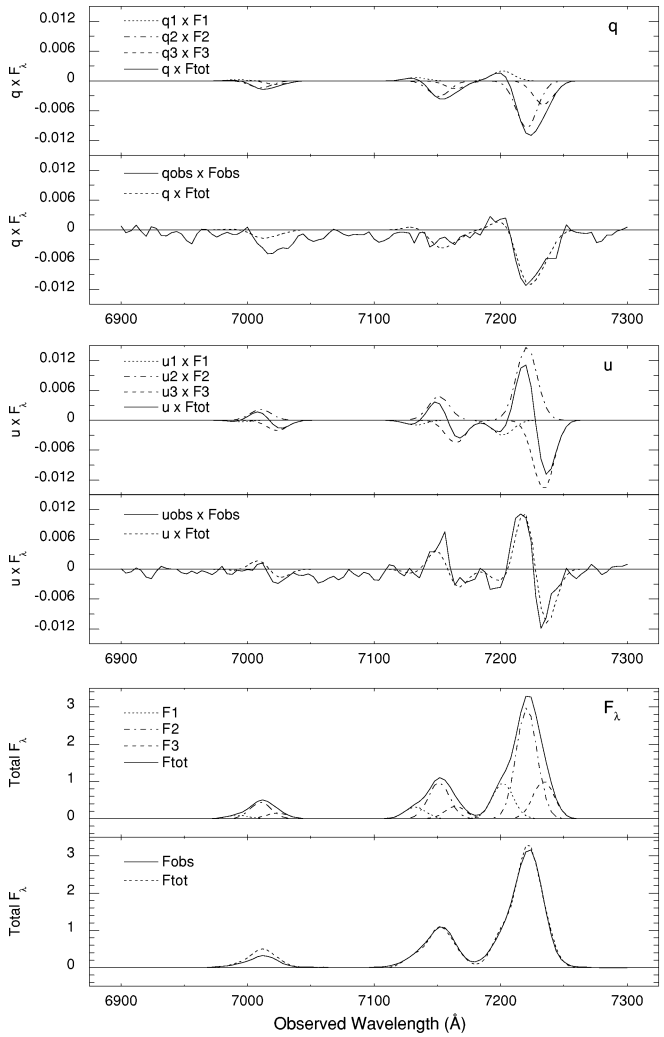

FIG. 7.—Our determination of the polarization components of the narrow-line emission. The fits assume that all narrow lines for a given component share the same polarizations. The ratio of [O III] λ5007/[O III] λ4959 = 3 for each component. The narrow lines were unresolved and assumed (Gaussian) widths to be that of the instrumental profile FWHM = 8.2 Å. Shown are the (continuum-subtracted) relative flux density F_λ and the rotated Stokes flux densities $q' \times F_\lambda$ and $u' \times F_\lambda$ (see Appendix and Table 2).

REFERENCES

Antonucci, R. R. J. 1993, ARA&A, 31, 473
Antonucci, R. R. J., & Miller, J. S. 1985, ApJ, 297, 621
Armus, L., et al. 1999, in preparation
Arribas, S., Mediavilla, E., & Garcia-Lorenzo, B. 1996, ApJ, 463, 509
Barthel, P. D. 1989, ApJ, 336, 606
Biretta, J., & Sparks, W. 1995, WFPC2 Instrument Science Report 95-01 (Baltimore: STScI)
Boroson, T., & Green, R. 1992, ApJS, 80, 109
Brotherton, M. S., Tran, H. D., Van Breugel, W., Dey, A., & Antonucci, R. R. J. 1997, ApJ, 487, L113
Brown, J. C., & McLean, I. S. 1977, A&A, 57, 141
Capetti, A., Macchetto, F. D., & Lattanzi, M. G. 1997, ApJ, 476, L67
Clarke, D., & Stewart, B. G. 1986, Vistas Astron., 29, 27
Cohen, M. H., Ogle, P. M., Tran, H. D., Vermeulen, R. C., Miller, J. S., Goodrich, R. W., & Martel, A. R. 1995, ApJ, 448, L77
Crawford, C. S., & Vanderriest, C. 1996, MNRAS, 283, 1003
Cutri, R. M., Huchra, J. P., Low, F. J., Brown, R. L., & Vanden Bout, P. A. 1994, ApJ, 424, L65
de Grijp, M. H. K., Miley, G. K., Lub, J., & DeJong, T. 1985, Nature, 314, 240
di Serego Alighieri, S., Cimatti, A., & Fosbury, R. A. E. 1994, ApJ, 431, 123
di Serego Alighieri, S., Cimatti, A., Fosbury, R. A. E., & Hes, R. 1997, A&A, 328, 510
Evans, I. N., Ford, H. C., Kinney, A. L., Antonucci, R. R. J., Armus, L., & Caganoff, S. 1991, ApJ, 369, L27
Evans, A. E., Sanders, D. B., Cutri, R. M., Radford, S. J. E., Surace, J. A., Solomon, P. M., Downes, D. & Kramer, C. 1998, ApJ, 506, 205
Fabian, A. C., & Crawford, C. S. 1995, MNRAS, 274, L63
Fanaroff, B. L., & Riley, J. M. 1974, MNRAS, 167, 3
Francis, P. J., Hewitt, P. C., Foltz, C. B., & Chaffee, F. H. 1992, ApJ, 398, 476
Garrington, S. T., Leahy, J. P., Conway, R. G., & Laing, R. A. 1988, Nature, 331, 147
Glenn, J., Schmidt, G. D., & Foltz, C. B. 1994, ApJ, 434, L47
Goodrich, R. W. 1992, ApJ, 399, 50
Goodrich, R. W., & Miller, J. S. 1995, ApJ, 448, L73
Goodrich, R. W., Miller, J. S., Martel, A., Cohen, M. H., Tran, H. D., Ogle, P. M., & Vermeulen, R. C. 1996, ApJ, 456, L9
Granato, G. L., Danese, L., & Franceschini, A. 1996, ApJ, 460, L11
Grandi, S. A. 1981, ApJ, 251, 451
Hall, P. B., Ellingson, E., & Green, R. F. 1997, AJ, 113, 1179
Hill, G. J., & Lilly, S. J. 1991, ApJ, 367, 1
Hines, D. C., Low, F. J., Evans, A. S., Scoville, N. Z., Rieke, M., Thompson, R. I., & Schneider, G. 1999, in preparation
Hines, D. C., & Schmidt, G. D. 1997, in ASP Conf. Ser. 128, Mass Ejection from AGN, ed. N. Arav, I. Shlosman, & R. J. Weymann (San Francisco: ASP), 59
Hines, D. C., Schmidt, G. D., Smith, P. S., Cutri, R. M., & Low, F. J. 1995, ApJ, 450, L1
Hines, D. C., & Wills, B. J. 1993a, ApJ, 415, 82 (HW93)
———. 1993b, Rev. Mexicana Astron. Astrophys., 27, 149
———. 1995, ApJ, 448, L69
Hutchings, J. B., & Neff, S. G. 1988, AJ, 96, 1575
Kennicutt, R. C. 1992, ApJS, 79, 255
Kleinmann, S. G., Hamilton, D., Keel, W. C., Wynn-Williams, C. G., Eales, S. A., Becklin, E. E., & Kuntz, K. D. 1988, ApJ, 328, 161 (K88)
Laing, R. A. 1988, Nature, 331, 149
Low, F. J., Cutri, R. M., Kleinmann, S. G., & Huchra, J. P. 1989, ApJ, 340, L1
Low, F. J., & Hines, D. C. 1999, in Astrophysics with Infrared Surveys: A Prelude to SIRTF, in press
Maloney, P. R., Begelman, M. C., & Pringle, J. E. 1996, ApJ, 472, 582
Manzini, A., & di Serego Alighieri, S. 1996, A&A, 311, 79
Miller, J. S., & Goodrich, R. W. 1990, ApJ, 355, 456
Miller, J. S., Robinson, L. B., & Goodrich, R. W. 1988, in Proc. 9th Santa Cruz Summer Workshop, Instrumentation for Ground-based Optical Astronomy, ed. L. B. Robinson (NY: Springer), 157
Mulchaey, J. S., Koratkar, A., Ward, M. J., Wilson, A. S., Whittle, M., Antonucci, R. R. J., Kinney, A. L., & Hurt, T. 1994, ApJ, 436, 586
Neugebauer, G., Miley, G. K., Soifer, B. T., & Clegg, P. E. 1986, AJ, 308, 815
O'Donoghue, A. A., Eilek, J. A., & Owen, F. N. 1990, ApJS, 72, 750
Ogle, P. M. 1997, in ASP Conf. Ser. 128, Mass Ejection from AGN, ed. N. Arav, I. Shlosman, & R. J. Weymann (San Francisco: ASP), 78
Oke, J. B., Bertola, F., & Capaccioli, M. 1981, ApJ, 243, 453
Ohta, K., Yamada, T., Nakanishi, K., Ogasaka, Y., Kii, T., & Hayashida, K. 1996, ApJ, 458, L570
Packham, C., Young, S., Hough, J. H., Axon, D. J., & Bailey, J. A. 1997, MNRAS, 288, 375
Pei, Y. C. 1992, ApJ, 395, 130
Pier, E. A., & Krolik, J. H. 1992, ApJ, 401, 99
Pogge, R. W. 1988, ApJ, 328, 519
Sanders, D. B. 1992, in ASP Conf. Ser. 31, Relationships between Active Galactic Nuclei and Starburst Galaxies, ed. A. V. Filippenko (San Francisco: ASP), 303
Sanders, D. B., Phinney, E. S., Neugebauer, G., Soifer, B. T., & Matthews, K. 1989, ApJ, 347, 29
Sanders, D. B., Soifer, B. T., Elias, J., Madore, B., Matthews, K., Neugebauer, G., & Scoville, N. 1988a, ApJ, 325, 74
Sanders, D. B., Soifer, B. T., Elias, J. H., Neugebauer, G., & Matthews, K. 1988b, ApJ, 328, L35
Schmidt, G. D., Angel, J. R. P., & Beaver, E. A. 1978, ApJ, 219, 477
Schmidt, G. D., Elston, R., & Lupie, O. L. 1992, AJ, 104, 1563
Schmidt, G. D., Hines, D. C., & Smith, P. S. 1997, in ASP Conf. Ser. 128, Mass Ejection from AGN, ed. N. Arav, I. Shlosman, & R. J. Weymann (San Francisco: ASP), 106
Schmidt, G. D., Stockman, H. S., & Smith, P. S. 1992, ApJ, 398, L57
Schmidt, G. D., Weymann, R. J., & Foltz, C. B. 1989, PASP, 101, 713
Schmidt, M., & Green, R. F. 1983, ApJ, 269, 352
Simmons, J. F. L., & Stewart, B. G. 1985, A&A, 142, 100
Soifer, B. T., Neugebauer, G., Armus, L., & Shupe, D. L. 1996, AJ, 111, 649
Storchi-Bergmann, T., Mulchaey, J. S., & Wilson, A. S. 1992, ApJ, 395, L73
Surace, J. A., Sanders, D. B., Vacca, W. D., Veilleux, S., & Mazzarella, J. M. 1998, ApJ, 492, 116
Taniguchi, Y., Sato, Y., Kawara, K., Murayama, T., & Mouri, H. 1997, A&A, 318, L1
Tran, H. D. 1995, ApJ, 440, 597
Ulvestad, J. S., Neff, S. G., & Wilson, A. S. 1987, AJ, 93, 22
Urry, M. C., & Padovani, P. 1995, PASP, 107, 803
Wilkes, B. J., Schmidt, G. D., Smith, P. S., Mathur, S., & McLeod, K. K. 1995, ApJ, 455, L13
Wills et al. 1999, in preparation
Wills, B. J., & Hines, D. C. 1997, in ASP Conf. Ser. 128, Mass Ejection from AGN, ed. N. Arav, I. Shlosman, & R. J. Weymann (San Francisco: ASP), 99
Wills, B. J., Netzer, H., & Wills, D. 1985, ApJ, 288, 94
Wills, B. J., Wills, D., Evans, N. J., Natta, A., Thompson, K. L., Breger, M., & Sitko, M. L. 1992, ApJ, 400, 96
Young, S., Hough, J. H., Efstathiou, A., Wills, B. J., Bailey, J. A., Ward, M. J., & Axon, D. J. 1996a, MNRAS, 281, 1206
Young, S. Packham, A. C., Hough, A. J. H., & Efstathiou, A. 1996b, MNRAS, 283, L1